# Theoretical model of x-ray scattering as a dense matter probe

G. Gregori[1] S. H. Glenzer[1] W. Rozmus[2] R. W. Lee[1] and O. L. Landen[1]
[1]*Lawrence Livermore National Laboratory, University of California, P.O. Box 808, Livermore, California 94551*
[2]*Department of Physics, University of Alberta, Edmonton, Alberta, Canada T6G 2J1*
(Received 11 September 2002; published 19 February 2003)

We present analytical expressions for the dynamic structure factor, or form factor $S(k,\omega)$, which is the quantity describing the x-ray cross section from a dense plasma or a simple liquid. Our results, based on the random phase approximation for the treatment on the charged particle coupling, can be applied to describe scattering from either weakly coupled classical plasmas or degenerate electron liquids. Our form factor correctly reproduces the Compton energy down-shift and the known Fermi-Dirac electron velocity distribution for $S(k,\omega)$ in the case of a cold degenerate plasma. The usual concept of scattering parameter is also reinterpreted for the degenerate case in order to include the effect of the Thomas-Fermi screening. The results shown in this work can be applied to interpreting x-ray scattering in warm dense plasmas occurring in inertial confinement fusion experiments or for the modeling of solid density matter found in the interior of planets.

DOI: 10.1103/PhysRevE.67.026412 PACS number(s): 52.70.La, 71.10.Ca, 61.10.Eq, 52.38.−r

## I. INTRODUCTION

Scattering by free electrons (Thomson scattering) in a plasma using optical probes has been a successful technique in studying basic parameters and transport properties in underdense plasmas with electron densities up to $n_e \lesssim 10^{21}$ cm$^{-3}$ [1]. However, in inertial confinement fusion (ICF) experiments a variety of plasma regimes are created [2], and the emerging interest in understanding the properties of matter under extreme conditions necessitates the development of accurate dense matter probes well above the critical densities achieved by optical techniques. The possibility of extending spectrally resolved Thomson scattering in the hard x-ray regime for the measurement of electron temperature, electron density, and ionization state of solid density plasmas was first discussed by Landen *et al.* [3] as a viable diagnostics alternative in ICF experiments, thus allowing the prospect of equation of state (EOS) model validation by an accurate determination of the microscopic electronic state of the material.

In Ref. [3], calculations were presented for scattering parameters $\alpha = 1/k\lambda_D \ll 1$, where $\lambda_D$ is the Debye length and $\mathbf{k} = \mathbf{k}_0 - \mathbf{k}_1$ is the difference between the wave number of the scattered and the incident probe radiation. In the present work, we provide a theoretical expression for the scattering form factor to represent elastic and inelastic x-ray scattering for arbitrary $\alpha$ parameter. Differently from the usual optical Thomson scattering, at hard x-ray wavelengths, both free and bound electrons in a plasma contribute to the scattering process, and, at the same time, the energy transferred by the photon to the electron is large compared to the kinetic energy. The scattered photons are thus down-shifted in energy by the Compton effect, but they are also broadened due to the thermal motion of the electrons. Since traditional Compton scattering usually denotes the scattering of x rays from rest electrons, while Thomson scattering refers to the scattering of photons by free charges in the low photon energy limit, in this paper we will use the term *x-ray Thomson scattering* to refer to the combined scattering by free and bound charges at arbitrary photon and electron energy.

Our treatment can be applied in the description of scattering from degenerate to weakly coupled plasmas. For plasmas obeying the classical statistics, the electron-electron coupling constant is defined as (see, e.g., Ichimaru [4]) $\Gamma = e^2/4\pi\epsilon_0 k_B T_e d$, where $T_e$ is the electron temperature and $d = (3/4\pi n_e)^{1/3}$ is the mean sphere radius per electron, with $n_e$ the electron density. In other words, $\Gamma$ is the ratio between the potential and the kinetic energy of the electrons. For coupling between different charged particles, we also need to account for the ionization state of the material. In an ideal plasma, $\Gamma \ll 1$ and the kinetic energy dominates the particle motion with negligible interparticle coupling, while in a strongly coupled plasma, $\Gamma \gg 1$, the electrostatic (Coulomb) forces determine the nature of the particle motion. Weakly coupled plasmas lie in the range $\Gamma \lesssim 1$. The extension of definition of the coupling constant $\Gamma$ to the quantum domain (i.e., a degenerate plasma) is discussed by Liboff [5]. In this case, quantum diffraction prevents the electrons to get arbitrarily close to each other and $\Gamma$ is now the ratio between the potential and the Fermi energy, $E_F = k_B T_F$, of the electrons. Having $E_F = \hbar^2 (3\pi^2 n_e)^{2/3}/2m_e$, as electron density increases, in contrast to a classical plasma, the coupling constant decreases, since $\Gamma \equiv \Gamma_q = e^2/4\pi\epsilon_0 E_F d \sim n_e^{-1/3}$.

## II. THEORY

### A. Basic definitions

We are interested in describing the scattering from a uniform plasma containing $N$ ions per unit volume. If $Z_A$ is the nuclear charge of the ion, the total number of electrons per unit volume in the system, including free and bound ones, is $Z_A N$. Let us now assume that we probe such a system with x rays of frequency $\omega_0$ such that $\hbar\omega_0 \gg E_I$, with $E_I$ the ionization energy of any bound electron, i.e., the incident frequency must be large compared to any natural absorption frequency of the scattering atom, which allows us to neglect photoabsorption. During the scattering process, the incident photon transfers momentum $\hbar\mathbf{k}$ and energy $\hbar\omega = \hbar^2 k^2/2m_e = \hbar\omega_0 - \hbar\omega_1$ to the electron, where $\omega_1$ is the frequency of

 

the scattered radiation. Under these conditions we can distinguish between electrons that are *kinematically* free with respect to the scattering process and *core* electrons that are tightly bound to the atom. If $a_n$ is the orbital radius of the electron with principal quantum number $n$, kinematically free electrons satisfy the relation [6,7] $ka_n \gtrsim 1$ (in the hydrogenic approximation, $a_n \sim a_B n^2/Z_A$ with $a_B = 4\pi\epsilon_0\hbar^2/m_e e^2$ the Bohr radius), while the opposite inequality applies for core electrons. This condition is equivalent to assuming that $\hbar\omega$, the energy transferred to the electron by Compton scattering, is larger than its binding energy. In the nonrelativistic limit ($\hbar\omega \ll \hbar\omega_0$)

$$k = |\mathbf{k}| = \frac{4\pi}{\lambda_0}\sin(\theta/2), \tag{1}$$

with $\lambda_0$ the probe wavelength and $\theta$ the scattering angle. We denote with $Z_f$ and $Z_c$ the number of kinematically free and core electrons, respectively. Clearly, $Z_A = Z_f + Z_c$. To avoid possible confusions, we should stress that $Z_f$ is conceptually different from the *true* ionization state of the atom. It includes both the truly free (removed from the atom by ionization) and the valence (weakly bound) electrons; thus $Z_f = Z + Z_v$, where $Z$ is the number of electrons removed from the atom, and $Z_v$ is the number of valence electrons. In the limiting case of a liquid metal, $Z = 0$, and only the valence (or conduction) electrons need to be considered.

### B. Scattering cross section

Following the approach of Chihara [8,9], the scattering cross section is described in terms of the dynamic structure factor of all the electrons in the plasma,

$$\frac{d^2\sigma}{d\Omega d\omega} = \sigma_T \frac{k_1}{k_0} S(k,\omega), \tag{2}$$

where $\sigma_T$ is the usual Thomson cross section and $S(k,\omega)$ is the total dynamic structure factor defined as

$$S(k,\omega) = \frac{1}{2\pi N}\int e^{i\omega t}\langle \rho_e(\mathbf{k},t)\rho_e(-\mathbf{k},0)\rangle dt, \tag{3}$$

with $\langle \cdots \rangle$ denoting an ensemble average and

$$\rho_e(\mathbf{k},t) = \sum_{s=1}^{Z_A N} \exp[i\mathbf{k}\cdot\mathbf{r}_s(t)] \tag{4}$$

is the Fourier transform of the total electron density distribution, with $\mathbf{r}_s(t)$ the time dependent position vector of the $s$th electron. Assuming that the system is isotropic, as in the case of interest here (liquid metals or plasmas), the dynamic structure factor depends only on the magnitude of $k$, not on its direction. The next step consists in separating the total density fluctuation, Eq. (4), between the free ($Z_f$) and core ($Z_c$) electron contributions, and separating the motion of the electrons from the motion of the ions. The details of procedure are given by Chihara [8,9], thus obtaining for the dynamic structure,

$$S(k,\omega) = |f_I(k) + q(k)|^2 S_{ii}(k,\omega) + Z_f S^0_{ee}(k,\omega) + Z_c \int \tilde{S}_{ce}(k,\omega-\omega') S_s(k,\omega') d\omega'. \tag{5}$$

The first term in Eq. (5) accounts for the density correlations of electrons that dynamically follow the ion motion. This includes both the core electrons, represented by the ion form factor $f_I(k)$, and the screening cloud of free (and valence) electrons that surround the ion, represented by $q(k)$ [10]. $S_{ii}(k,\omega)$ is the ion-ion density correlation function. The second term in Eq. (5) gives the contribution in the scattering from the free electrons that do not follow the ion motion. Here, $S^0_{ee}(k,\omega)$ is the high frequency part of the electron-electron correlation function [11] and it reduces to the usual electron feature [12,13] in the case of an optical probe. Inelastic scattering by core electrons is included in the last term of Eq. (5), which arises from Raman transitions to the continuum of core electrons within an ion, $\tilde{S}_{ce}(k,\omega)$, modulated by the self-motion of the ions, represented by $S_s(k,\omega)$. We point out that in Eq. (5) electron-ion correlations are implicitly accounted in the first term, since, as shown by Chihara [8], the electron-ion response function can be written in terms of the ion-ion response function. We observe that the total density correlation function must obey the relation [14]

$$S(k,-\omega) = \exp(-\hbar\omega/k_B T_e) S(k,\omega), \tag{6}$$

which is a consequence of detailed balance. This gives rise to asymmetry in the spectrum as we will discuss further in the following sections.

We will present simplified expressions for each term in Eq. (5). The relative importance of each term is discussed and scattering profiles for typical conditions found in experiments are obtained. The sensitivity to the various parameters is presented using beryllium solid density plasma as an example. A similar method based on the measurement of frequency-integrated (total) x-ray cross section for the diagnostics of high density plasmas was originally proposed by Nardi and co-workers [10,15,16]. While their approach was based on the calculation of the static structure factor, we wish to determine the dynamic structure factor. This requires frequency resolved measurements, standard in optical Thomson scattering. The various terms in Eq. (5) provide scattering signals at different frequencies. With the available x-ray line sources, spectrometers and detectors in ICF experiments [3], we currently are able to resolve the high frequency part of the spectrum, $\omega \gtrsim k v_t$, where $v_t = (k_B T_e/m_e)^{1/2}$ is the electron thermal speed.

### C. Ion correlations: The ion feature

The ion-ion correlations reflect the thermal motion of the ions and/or the ion plasma frequency, and since we cannot currently experimentally access this low frequency part of the spectrum, we can approximate $S_{ii}(k,\omega) = S_{ii}(k)\delta(\omega)$. We thus only need to calculate the static structure factor for ion-ion correlations. We shall also observe that for typical conditions in dense plasmas for ICF experiments, the ions are always nondegenerate, since their thermal de Broglie

wavelength is much smaller than the average interparticle distance. On the other hand, the electrons can exhibit some degree of degeneracy, and in the case of very cold and dense plasmas, they will obey the Fermi-Dirac distribution. Under these conditions, and within the framework of the random phase approximation (RPA), we can calculate $S_{ii}(k)$ using the semiclassical approach suggested by Arkhipov and Davletov [17], which is based on a pseudopotential model for the interaction between charged particles to account for quantum diffraction effects (i.e., the Pauli exclusion principle) and symmetry [18]. The correlation function is then calculated at the effective temperature $T_{cf} \simeq (T_e^2 + T_q^2)^{1/2}$, where $T_q = T_F/(1.3251 - 0.1779\sqrt{r_s})$, with $r_s = d/a_B$. This corrected temperature is chosen such that the temperature of an electron liquid obeying classical statistics exactly gives the same correlation energy of a degenerate quantum fluid at $T_e = 0$ obtained from quantum Monte Carlo calculations [19]. This approach was shown to reproduce finite-temperature static response of an electron fluid, valid for arbitrary degeneracy [19].

The resultant expressions for the various static structures are thus

$$S_{rs}(k) = \delta_{rs} - \frac{\sqrt{n_r n_s}}{k_B T_{cf}} \Phi_{rs}(k), \tag{7}$$

where $r,s = e$ (electrons) or $i$ (ions), $n_e = Z_f n_i = Z_f N$, and the temperature has been assumed equal for both ions and electrons. Symmetry in the electron-ion interactions requires $S_{ei}(k) = S_{ie}(k)$. The coefficients $\Phi_{rs}(k)$ are given by [17]

$$\Phi_{ee}(k) = \frac{e^2}{\epsilon_0 \Delta}\left[\frac{k^2}{1+k^2\lambda_{ee}^2} + k_{Di}^2\left(\frac{1}{(1+k^2\lambda_{ee}^2)(1+k^2\lambda_{ii}^2)} - \frac{1}{(1+k^2\lambda_{ei}^2)^2}\right) + A\left(k^2 + \frac{k_{Di}^2}{1+k^2\lambda_{ii}^2}\right)k^2 \times \exp(-k^2/4b)\right], \tag{8}$$

$$\Phi_{ii}(k) = \frac{Z_f^2 e^2}{\epsilon_0 \Delta}\left[\frac{k^2}{1+k^2\lambda_{ii}^2} + k_{De}^2\left(\frac{1}{(1+k^2\lambda_{ee}^2)(1+k^2\lambda_{ii}^2)} - \frac{1}{(1+k^2\lambda_{ei}^2)^2}\right) + \frac{Ak^2 k_{De}^2}{1+k^2\lambda_{ii}^2}\exp(-k^2/4b)\right], \tag{9}$$

$$\Phi_{ei}(k) = -\frac{Z_f e^2}{\epsilon_0 \Delta}\frac{k^2}{1+k^2\lambda_{ei}^2}, \tag{10}$$

where $b = (\lambda_{ee}^2 \pi \ln 2)^{-1}$, $A = k_B T_{cf} \ln 2 \pi^{3/2} b^{-3/2} \epsilon_0 / e^2$, and

$$\Delta = k^4 + \frac{k^2 k_{De}^2}{1+k^2\lambda_{ee}^2} + \frac{k^2 k_{Di}^2}{1+k^2\lambda_{ii}^2} + k_{De}^2 k_{Di}^2\left(\frac{1}{(1+k^2\lambda_{ee}^2)(1+k^2\lambda_{ii}^2)} - \frac{1}{(1+k^2\lambda_{ei}^2)^2}\right) + Ak^2 k_{De}^2\left(k^2 + \frac{k_{Di}^2}{1+k^2\lambda_{ii}^2}\right)\exp(-k^2/4b). \tag{11}$$

The inverse of the electron and the ion Debye lengths are $k_{De} = (n_e e^2/\epsilon_0 k_B T_{cf})^{1/2}$ and $k_{Di} = (Z_f n_e e^2/\epsilon_0 k_B T_{cf})^{1/2}$, respectively. In Eqs. (8)–(11), the thermal de Broglie wavelength is defined by $\lambda_{rs} = \hbar/(2\pi\mu_{rs} k_B T_{cf})^{1/2}$ with $\mu_{rs} = m_r m_s/(m_r + m_s)$ the reduced mass of the interacting pair. To complete the description of the first term of Eq. (5) we need to calculate the screening charge and the ionic form factor. The screening charge is given by [8,17]

$$q(k) = \frac{C_{ei}(k)}{\epsilon(k,0)}, \tag{12}$$

where $\epsilon(k,0)$ is the electron permittivity at frequency $\omega = 0$, which is calculated including the full effect of different statistics (Boltzmann or Fermi-Dirac) as we will discuss in the following section, and $C_{ei}(k)$ the electron-ion direct correlation function. Using the Ornstein-Zernike relations [14], the electron-ion direct correlation is found to be

$$C_{ei}(k) = \frac{\sqrt{Z_f} S_{ei}(k)}{S_{ee}(k) S_{ii}(k) - S_{ei}^2(k)}, \tag{13}$$

with the partial static structures given by Eq. (7).

The ionic form factor, $f_I(k)$, can be exactly calculated, for example, following the approach described by James [20] in the Hartree-Fock self-consistent field method. This approach may be quite laborious, so, instead, hydrogenic wave functions with inclusion of appropriate screening constants for the bound electrons [21] have been used to obtain the ionic form factor. As shown by Pauling and Sherman [21], this technique is fairly accurate for the low-$Z$ elements with the advantage of simple analytical results. Typically, the contribution from $K$-shell ($1s$) electrons to the total $f_I(k)$ is given by

$$f_{I,1s}(k) = \frac{1}{[1 + (k a_s/2)^2]^2} \quad \text{per } K \text{ electron}, \tag{14}$$

where $a_s = a_B/(Z_A - z_{scr})$ is the effective radius of the electron, which is itself screened by the other $1s$ electron. The size screening constant, $z_{scr}$, varies for each element and its value can be found in Ref. [21]. Contributions to the ionic form factor from upper level bound electrons can be calculated similarly and formulas are given in Ref. [21]. For neutral isolated atoms, the ionic form factor is replaced by the atomic form factor $f_A(k)$, which is obtained for various elements, for example, from the numerical fits given by Waasmaier and Kirfel [22]. However, for plasmas and liquid met-

als, the approximation $f_A(k) \sim f_I(k) + q(k)$ is expected to strictly hold only in the limit [23] $k \to 0$, thus giving $f_A(k) = f_I(k) + q(k) = Z_c + Z_f = Z_A$.

### D. Electron correlations: The electron feature

The free electron density-density correlation function that appears in the second term of Eq. (5) can be formally obtained through the fluctuation-dissipation theorem [24]:

$$S^0_{ee}(k,\omega) = -\frac{\hbar}{1-\exp(-\hbar\omega/k_B T_e)} \frac{\epsilon_0 k^2}{\pi e^2 n_e} \mathrm{Im}\left[\frac{1}{\epsilon(k,\omega)}\right], \tag{15}$$

where $\epsilon(k,\omega)$ is the electron dielectric response function. In the case of an ideal classical plasma, the dielectric response is evaluated from a perturbation expansion of the Vlasov equation [25]. The resultant form for the density correlation function is then known as the Salpeter electron feature [12]. This approach, however, fails when the electrons become degenerate or nearly degenerate as quantum effects begin to dominate. Under the assumption that interparticle interactions are weak, so that the nonlinear interaction between different density fluctuations is negligible, the dielectric function can be derived in the RPA [26,27]. In the classical limit, it reduces to the usual Vlasov equation.

We shall stress the point that in the limit of the RPA, strong coupling effects are not accounted for, thus limiting the model validity to plasma conditions in the range $\Gamma \lesssim 2$. Use of the RPA at larger couplings may still provide fairly accurate results if $kd \gtrsim 1$ [28,29]. In the cases studied here, the plasmas are within the range of validity. However, extensions to strong coupling are possible in terms of a local field correction [30] of the dielectric response functions, but they are significantly more complex and can be obtained only through the solution of the hypernetted chain equation [31] or molecular dynamics simulations [32]. It turns out that the RPA is also rather accurate to describe the collective behavior of the electrons in the valence band of metals [33,34], even if higher-order corrections beyond the RPA have been observed in some experiments [35,36]. In those cases, deviations from the RPA resulted from the periodic potential of the crystal structure of the solid or from higher-order density excitations [37].

The RPA form of the dielectric function is (see, e.g., Landau *et al.* [25])

$$\epsilon(k,\omega) = 1 - \frac{e^2}{\hbar\epsilon_0 k^2} \int \frac{f(\mathbf{p}+\hbar\mathbf{k}/2) - f(\mathbf{p}-\hbar\mathbf{k}/2)}{\mathbf{k}\cdot\mathbf{p}/m_e - \omega - i\nu} \frac{2d^3p}{(2\pi\hbar)^3}, \tag{16}$$

with $\nu \to 0^+$. The electron distribution function is specified as

$$f(\mathbf{p}) = \frac{1}{\exp\left(\dfrac{p^2/2m_e - \mu}{k_B T_e}\right) + 1}, \tag{17}$$

where $\mathbf{p}$ is the electron momentum and $\mu$ is the chemical potential, defined by the normalization condition

$$\int f(\mathbf{p}) \frac{2d^3p}{(2\pi\hbar)^3} = n_e, \tag{18}$$

where we have accounted for both spin-state electrons. A useful fitting formula for the chemical potential that interpolates between the classical and the quantum regions is [38]

$$\frac{\mu}{k_B T_e} = -\frac{3}{2}\ln\Theta + \ln\frac{4}{3\sqrt{\pi}} + \frac{A\Theta^{-b-1} + B\Theta^{-(b+1)/2}}{1 + A\Theta^{-b}}, \tag{19}$$

with $\Theta = k_B T_e / E_F$ ($E_F$ is the Fermi energy of the electrons), $A = 0.259\,45$, $B = 0.072$, and $b = 0.858$. In the limit $T_e \to 0$, which corresponds to an electron gas in the ground state, the dielectric function takes the Lindhard-Sommerfeld form [27]. In the case of scattering from uncorrelated electrons, the form of the dynamic structure follows the electron velocity distribution function [39] and it has been recently specialized to the case of x-ray scattering for conditions relevant to ICF experiments by Landen *et al.* [3].

Even for nondegenerate electrons, the classical result for the dynamic structure initially derived by Salpeter [12] cannot be directly applied to describe x-ray (Compton) scattering, since quantum corrections are not negligible anymore [40]. The importance of such effects is represented by the parameter

$$\kappa = \frac{\hbar k}{2\sqrt{2} m_e v_t}, \tag{20}$$

which is large if the classical Compton shift ($\hbar^2 k^2 / 2m_e$) is large compared to the average thermal energy of the electrons. By substituting in Eq. (16) the Boltzmann distribution and carrying out the integration in momentum space, we get [40]

$$\epsilon(k,\omega) = 1 + \frac{\omega_p^2}{k^2 v_t^2} \frac{1}{4\kappa}\left[\frac{1 - W(x_e + \kappa)}{x_e + \kappa} - \frac{1 - W(x_e - \kappa)}{x_e - \kappa}\right], \tag{21}$$

where

$$x_e = \frac{\omega}{\sqrt{2} k v_t}, \tag{22}$$

$$W(x_e) = 1 - 2x_e e^{-x_e^2} \int_0^{x_e} e^{t^2} dt + i\sqrt{\pi} x_e e^{-x_e^2}. \tag{23}$$

We will refer to this approach together with the fluctuation-dissipation theorem as the quantum corrected Salpeter approximation (QCSA). In the limit $\kappa \ll 1$, the usual Salpeter approximation is indeed reproduced [40]. The fact that the QCSA includes both the correction in the electron recoil energy and detail balance results in completely different line profiles than the ones expected from traditional (optical)

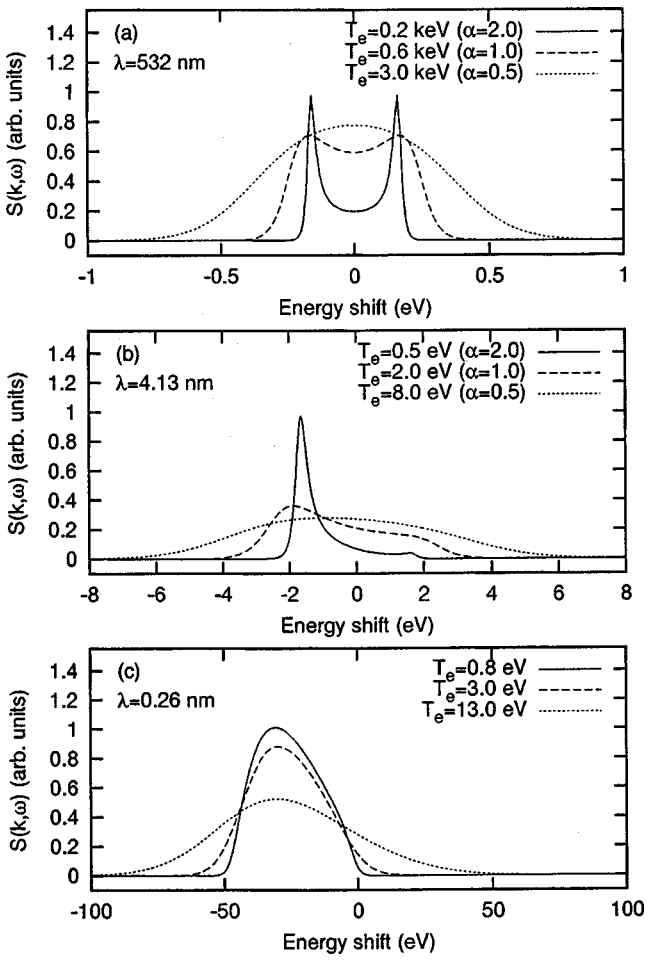


FIG. 1. Comparison between free electron dynamic structures $S^0_{ee}(k,\omega)$. (a) Optical probe in a classical plasma with density $n_e = 1.0\times 10^{19}$ cm$^{-3}$ and a scattering angle of $\theta = 90°$. The parameter $\alpha = 1/k\lambda_D$ is given for different electron temperatures. The Salpeter approximation applies in this regime. (b) EUV probe in a classical plasma with density $n_e = 1.0\times 10^{21}$ cm$^{-3}$ and a scattering angle of $\theta = 160°$. The parameter $\alpha = 1/k\lambda_D$ is given for different electron temperatures. The electron recoil energy is 0.3 eV and the QCSA is used in the calculation of the dynamic structure. (c) Hard x-ray probe in a degenerate plasma with density $n_e = 1.0\times 10^{23}$ cm$^{-3}$ and a scattering angle of $\theta = 60°$. The degenerate scattering parameter (see text) is now $\alpha = 0.8$ for $T_e = 0.8$ eV or $T_e = 3.0$ eV, and $\alpha = 0.5$ for $T_e = 13.0$ eV. The electron recoil energy is 22 eV and the full RPA is used in the calculation of the dynamic structure.

Thomson scattering. This is clearly seen in Fig. 1, where we compare typical line profiles for an incident optical probe at $\lambda_0 = 532$ nm, an extreme ultraviolet (EUV) probe at $\lambda_0 = 4.13$ nm, and a hard x-ray probe at $\lambda_0 = 0.26$ nm. For the optical probe, the Compton recoil energy ($\sim 10^{-5}$ eV) is always negligible compared to the electron thermal energy. Thus the Salpeter approximation gives for the free electron structure factor the well known symmetric satellites for large values of $\alpha = 1/k\lambda_D$. This is not true anymore at $\lambda_0 = 4.13$ nm, since the parameter $\kappa \gtrsim 1$ for $\alpha > 1$, and the resultant spectrum obtained from the QCSA exhibits strong asymmetries due to detailed balance. In particular, the red shifted component on the spectrum is strongly enhanced compared to the blue shifted one. When we move to the x-ray regime, since $\hbar\omega/k_B T_e \gg 1$, only the red part of the spectrum remains and the electron recoil energy mainly determines its location. As the electron temperature is reduced below $T_F$, the electron velocity distribution becomes degenerate and the full RPA is required to describe the spectral shape of the free electron correlation function. In Fig. 1(c), different profiles are plotted at the electron temperatures that give same classical scattering parameters $\alpha = 1/k\lambda_D$ as in the corresponding Figs. 1(a) and 1(b). It is then clear that, in this regime, the usual definition of the scattering parameter in terms of the Debye length breaks down. In oder to describe scattering processes in degenerate and strongly coupled fluids, we will introduce the *generalized* scattering parameter $\alpha = 1/ks$, where $s$ is the characteristic screening length of the electrostatic interactions. For an ideal classical plasma $s$ coincides with the Debye length $\lambda_D$. If $\alpha < 1$, the electrons behave as uncorrelated scatterers, while for large $\alpha$ parameters the scattering reflects their collective motion. In a classical plasma $\alpha \sim (T_e/n_e)^{1/2}$, and the nature of the scattering depends on both the electron temperature and the electron density. As the plasma becomes degenerate, the Debye length does not represent anymore the screening of the Coulomb forces. However, the classical results are still valid if, instead of using the kinetic temperature, they are evaluated at the effective temperature $T_{cf}$ [19], as defined in paragraph 2 of Sec. II C. Figure 2 shows $\alpha = $ const contours in the $T_e$-$n_e$ plane for typical experimental conditions. We see that in the case of an ideal ($r_s = d/a_B \to 0$) degenerate electron liquid this approximation yields $s \sim \lambda_{TF}$, where $\lambda_{TF} = \sqrt{2\epsilon_0 E_F/3n_e e^2}$ is the Thomas-Fermi screening length. Thus, $\alpha$ becomes proportional to $n_e^{1/6}$ and the type of scattering (uncorrelated or collective) is independent of $T_e$ and weakly dependent on the electron density. Collective scattering can thus only be practically accessed by increasing the wavelength of the probe x ray. Finally, in a strongly coupled plasma ($\Gamma \gg 1$), the mean particle separation $d$ is the only meaningful quantity that can be associated to a screening distance, thus $\alpha = 1/kd$. This gives a dependence $\alpha \sim n_e^{1/3}$, which smoothly interpolates between the ideal classical plasma and fully degenerate regimes.

In Fig. 3, we have plotted normalized line profiles of $S^0_{ee}(k,\omega)$ calculated assuming incident x rays with $\lambda_0 = 0.26$ nm, corresponding to the Ti He-$\alpha$ 4.75-keV emission line, and a scattering angle of $\theta = 160°$. The various models compared with the RPA in Fig. 3 are the analytical Lindhard-Sommerfeld theory [27], which is exact for $T_e = 0$, the QCSA form factor, and the calculations of Landen *et al.* [3], which are a direct representation of the electron distribution function. At a density of $n_e = 1.0\times 10^{23}$ cm$^{-3}$, the Fermi temperature is $T_F = 7.85$ eV. We indeed see that, at temperatures lower than $T_F$, when degeneracy effects are important, the QCSA result deviates from the RPA one. On the other hand, at $T_e = 10$ eV ($T_e > T_F$), the QCSA agrees very well with the RPA since now the kinetic temperature is comparable with $T_F$. From Fig. 3, we also see that at $T_e = 1$ eV the calculated profile of $S^0_{ee}(k,\omega)$ is parabolic, while at $T_e = 10$ eV the profile is Gaussian. The transition from a para-

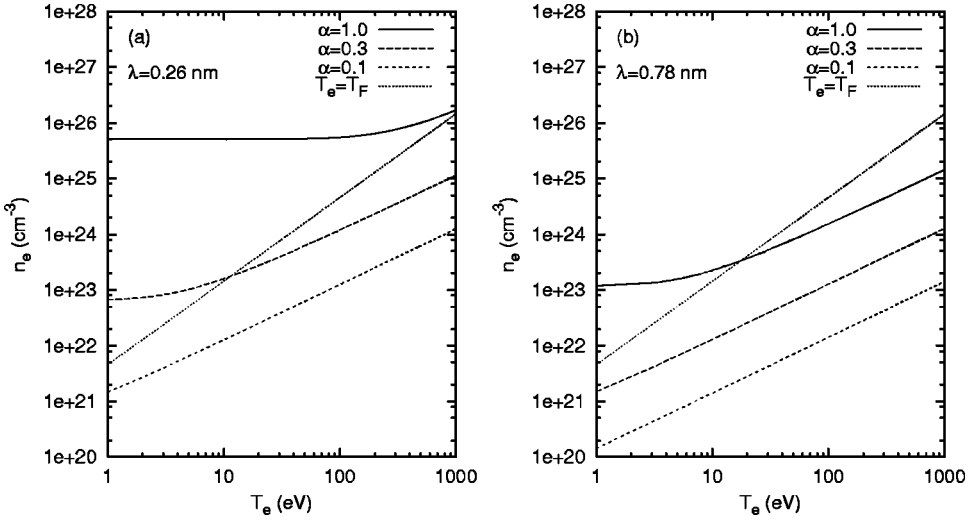


FIG. 2. Calculated $\alpha=$const contours for $\lambda_0=0.26$ nm (a) and $\lambda_0=0.78$ nm (b), and $\theta=160°$. The line $T_e=T_F$ is also plotted in the figure.

bolic to a Gaussian profile, as the electron temperature is raised, corresponds to the transition from Fermi to Boltzmann statistics in the electron velocity distribution [41]. Dynamic structures for collective scattering (i.e., large $\alpha$ parameters) are shown in Fig. 4, which correspond to a longer probe radiation of wavelength $\lambda_0=0.78$ nm (Al He-$\alpha$ 1.6-keV emission line), all the other conditions being the same as in Fig. 3. Again, we see failure of the QCSA for the degenerate case ($T_e \ll T_F$), but agreement with the RPA for $T_e \sim T_F$. In Figs. 3 and 4, we see the strong asymmetry with respect to $\omega=0$ in the line profiles resulting from the detailed balance relation (6). In Fig. 4(a), we also notice the departure from a typical parabolic to a linear profile of the degenerate electron fluid response. At $T_e=0$, this occurs when the Doppler broadening of the line ($\sim \hbar k v_F$, where $v_F$ is the Fermi velocity) is larger than the classical Compton shift ($\hbar^2 k^2/2m_e$). In this case, electrons at the lowest energy levels within the Fermi sphere cannot absorb the Compton energy, as it would still leave them inside the fully occupied Fermi sphere. Accounting for such a contribution that affects the region $\omega/k < v_F - \hbar k/2m_e$ yields a linear electron response for $T_e \ll T_F$ [27], as can be seen in Fig. 4(a).

### E. Core electron excitations

The last term in Eq. (5) corresponds to the density correlations of the tightly bound electrons within each single ion, and it arises from electron-hole and bound excitations of the inner core electrons. As discussed by Mizuno and Ohmura [7], inner core electrons can be excited by the probe radiation to continuum states and the corresponding spectrum of the scattered radiation is that of a Raman-type band. Experiments of Suzuki [42] have then confirmed the existence of such type of excitation in the form of a weak band near the tail of the Compton band. In the high frequency limit, the ion-ion self-structure is $S_s(k,\omega) \sim \delta(\omega)$ [14]. The Fermi *golden rule* in the first-order perturbation theory can be used to calculate the spectrum resulting from electron-hole excitations [43,44], thus obtaining the following for the $1s$ electron jumping into the continuum:

$$\tilde{S}_{ce}(k,\omega) \simeq \frac{256 r_k m_e a_s^2}{\hbar(1-e^{-2\pi/p_\omega a_s})} \frac{k^4 a_s^4 + k^2 a_s^2 (1+p_\omega^2 a_s^2)/3}{[(k^2 a_s^2 + 1 - p_\omega^2 a_s^2)^2 + 4 p_\omega^2 a_s^2]^3} \times \exp\left[ -\frac{2}{p_\omega a_s} \tan^{-1}\left( \frac{2 p_\omega a_s}{1 + k^2 a_s^2 - p_\omega^2 a_s^2} \right) \right], \quad (24)$$

where $a_s = a_B/Z_A$ is the $K$-shell radius, $r_k \sim 1 - (|f_l(k)|/Z_c)^2$ is a normalization factor, and $p_\omega$ is defined by the relation $\hbar^2 p_\omega^2/2m_e = \hbar\omega - E_B$, with $E_B$ the binding energy of the $K$-shell electron. Clearly, transitions into the continuum occurs only if $\hbar\omega > E_B$, thus, in contrast to the usual Compton scattering, the position of the Raman band is

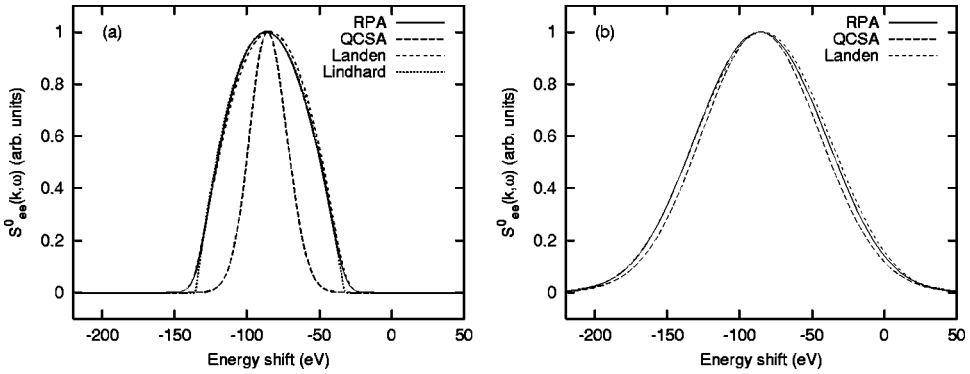


FIG. 3. Free electron dynamic structure $S^0_{ee}(k,\omega)$ for $n_e=1.0\times10^{23}$ cm$^{-3}$ at $T_e=1$ eV (a) and $T_e=10$ eV (b). The probe radiation is $\lambda_0=0.26$ nm and the scattering angle is $\theta=160°$, and $\alpha=0.40$ (a) or $\alpha=0.29$ (b). Values have been normalized to the same peak height to facilitate the comparison.

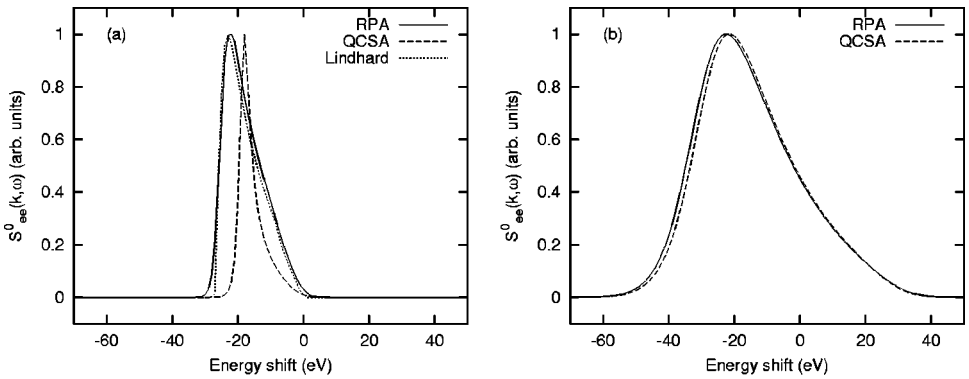


FIG. 4. Free electron dynamic structure $S^0_{ee}(k,\omega)$ for $n_e=1.0\times10^{23}$ cm$^{-3}$ at $T_e=1$ eV (a) and $T_e=10$ eV (b). The probe radiation is $\lambda_0=0.78$ nm and the scattering angle is $\theta=160°$, and $\alpha=1.17$ (a) or $\alpha=0.85$ (b). Values have been normalized to the same peak height to facilitate the comparison.

independent on $k$ (or the scattering angle), with its threshold determined only by the ionization threshold of the inner $K$ shell of the atom.

In Fig. 5, we compare the dynamic structure factors for free and core electrons, as given by Eqs. (15) and (24) for the case of a beryllium solid density plasma.

At $T_e=1$ eV, the $K$-shell ionization potential is chosen to be the same as for isolated beryllium atoms, while at $T_e=40$ eV the beryllium ions are assumed to be all doubly ionized with a $K$-shell threshold calculated from the fitting formula given by Band *et al.* [45]. In both cases we have assumed $Z_f=Z_c=2$. From Fig. 5, we clearly see that either considering an x-ray probe at $\lambda_0=0.26$ nm or $\lambda_0=0.78$ nm, the contribution from core electron transitions to the continuum is small compared to the free electron dynamic structure. In addition, the Raman band has width comparable or larger than the Compton band [46], so we can regard this type of contribution as yielding only a small background. This also seems consistent with the preliminary results presented by Glenzer [47] on x-ray scattering from moderately heated beryllium targets.

### III. X-RAY SCATTERING PROFILES

Based on the theory outlined in the preceding sections, we are now able to calculate the scattering profile for x-ray probes at arbitrary scattering angle, for either classical or quantum plasmas. The only limitation is that the degree of coupling must not be too large to invalidate the limits of the RPA. We have obtained synthetic line profiles for the Ti He-$\alpha$ 4.75-keV radiation probe at $\theta=160°$ scattering angle. In addition, we have assumed that the probe material consists of beryllium ($Z_A=4$) at various compressed densities. To simulate actual experimental data, the theoretical line profile from Eq. (5) has been convoluted with a 50-eV Gaussian instrument function. In Fig. 6, we have plotted synthetic line shapes for different values of $T_e$, $n_e$, and $Z_f$ (or $Z_c$). Figure 6(a) shows that the broadening of the Compton profile, above instrumental, goes as $\sqrt{T_F}\sim n_e^{1/3}$ at highest density. Similarly, Figs. 6(b) and 6(c) show an increased Doppler broadening of the Compton feature as $T_e$ is raised.

The effect of the ionization state on the line profiles can also be seen in Figs. 6(d)–6(f). Here, we have plotted synthetic line shapes for different values of $Z_f$ (or $Z_c$) with $n_e=3.0\times10^{23}$ cm$^{-3}$ ($T_F=16.3$ eV) and $T_e=1$ eV (d), $T_e=10$ eV (e), or $T_e=40$ eV (f). We see dramatic differences in the simulated line shapes for the various $Z_f$. This effect then suggests that x-ray Thomson scattering can also be implemented for inferring the ionization state of solid density plasmas based on the difference in the intensity between

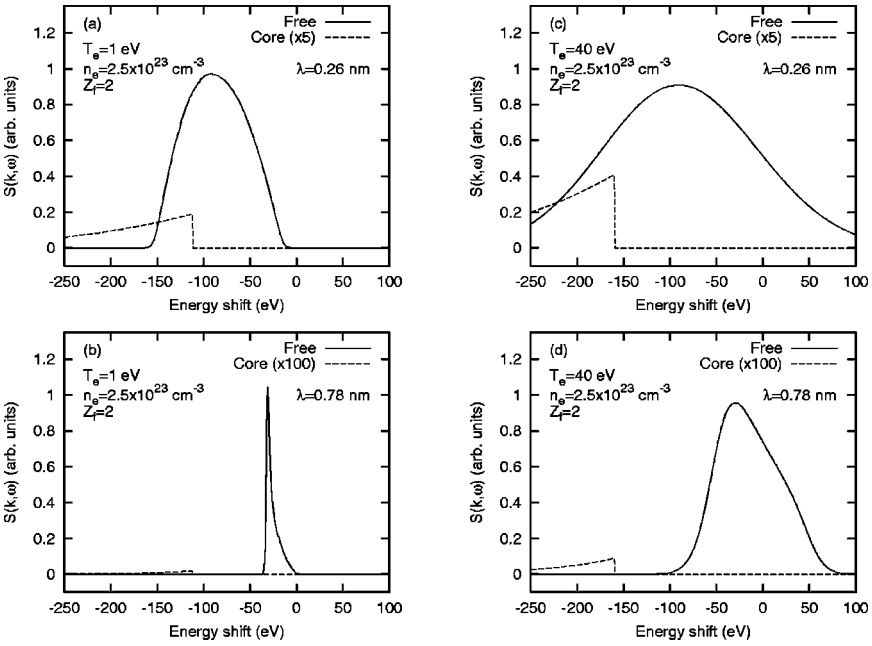


FIG. 5. Comparison between the RPA dynamic structures arising from free and core electrons for a beryllium plasma. At $T_e=1$ eV the beryllium is assumed in its normal state ($Z_f$ consists only of conduction electrons) with a $K$-shell ionization potential $E_B=111.5$ eV. At $T_e=40$ eV, the beryllium is assumed doubly ionized ($Z_f$ includes only free electrons) with $E_B=159.5$ eV. The scattering angle is $\theta=160°$. The scattering parameter is $\alpha=0.46$ (a), $\alpha=1.36$ (b), $\alpha=0.23$ (c), $\alpha=0.67$ (d).

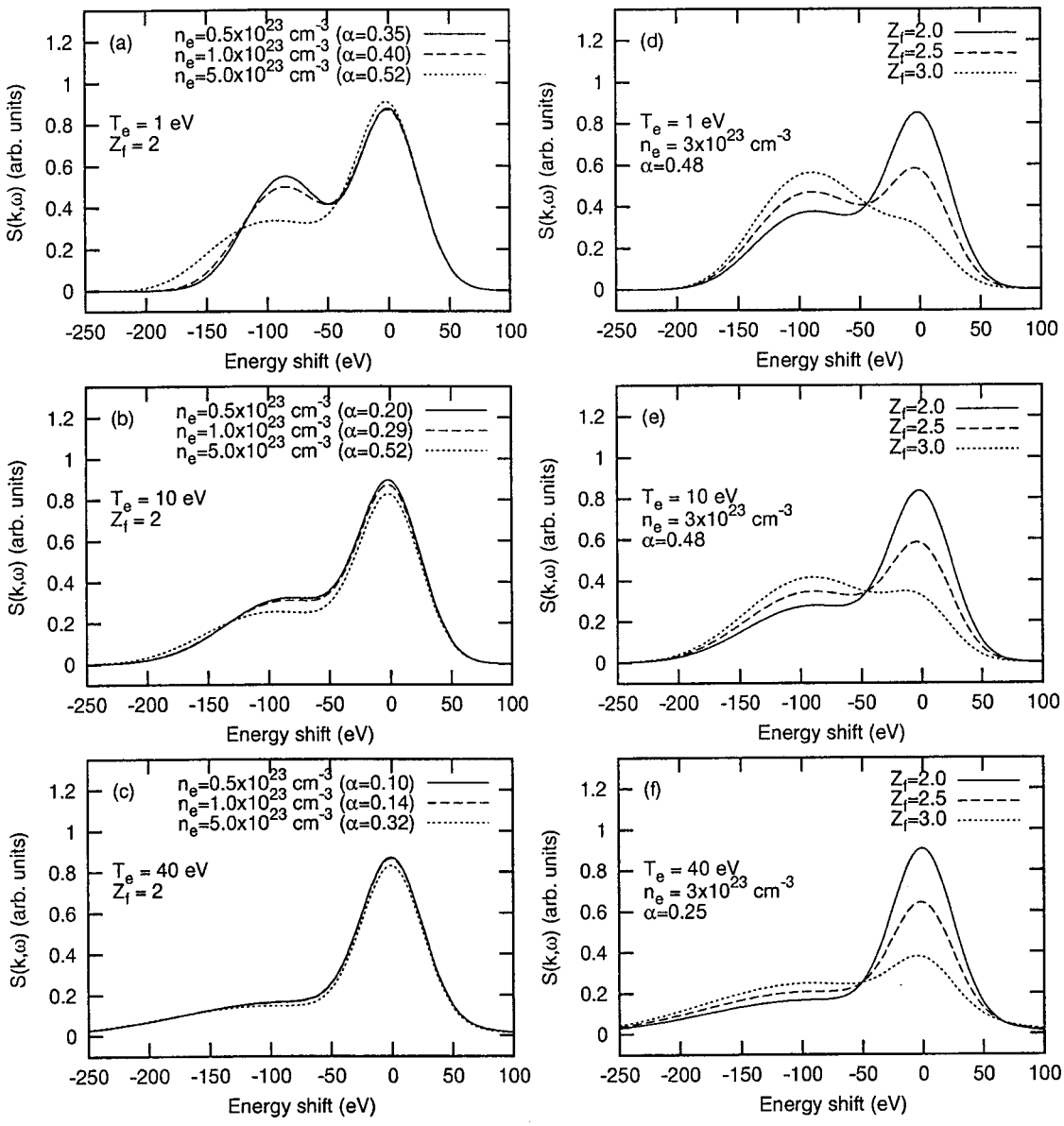


FIG. 6. Synthetic dynamic structure $S(k,\omega)$ calculated for beryllium target ($Z_A=4$) at various $T_e$, $n_e$, and $Z_f$. The probe radiation is $\lambda_0=0.26$ nm and scattering angle $\theta=160°$.

the unshifted and the Compton shifted peaks. This possibility was initially suggested by Landen *et al.* [3], since current optical techniques cannot directly measure the number of free electrons in dense plasmas. On the other hand, the ratio of the scattered intensities between the shifted and the unshifted peaks is only sensitive to $Z_f$ which is *not* the same as $Z$, the true ionization state of the material. Since $Z_f \gtrsim Z$, the measure of $Z_f$ will thus only provide an upper bound to $Z$, unless the number of valence electrons can be determined by other techniques. The ratio $I_e(k)/I_i(k)$ between the scattered intensity in the electron feature and in the ion feature is given in Table I, where

$$I_e(k)=Z_f\int_0^\infty S_{ee}^0(k,\omega)[1+\exp(-\hbar\omega/k_BT_e)]d\omega=Z_fS_{ee}^0(k) \tag{25}$$

and

$$I_i(k)=|f_I(k)+q(k)|^2S_{ii}(k). \tag{26}$$

Using the structure factors (7), we have [9]

$$S_{ee}^0(k)=S_{ee}(k)-\frac{|q(k)|^2}{Z_f}S_{ii}(k). \tag{27}$$

If $\alpha \ll 1$ and for weakly degenerate plasmas, $q(k)\ll 1$ and $S_{ee}^0(k)=S_{ee}(k)=S_{ii}(k)\sim 1$. Thus, in this limit

$$\frac{I_e(k)}{I_i(k)}\simeq\frac{Z_f}{|f_I(k)|^2}\gtrsim\frac{Z_f}{Z_c^2}. \tag{28}$$

In the case of Ti He-$\alpha$ 4.75-keV radiation probe at $\theta=160°$ scattering angle, the ratio $I_e(k)/I_i(k)$ is given in

TABLE I. Ratio between the scattered intensity in the electron feature, $I_e(k)$, and in the ion feature, $I_i(k)$. Beryllium target ($Z_A=4$) with probe radiation $\lambda_0=0.26$ nm and scattering angle $\theta=160°$.

| $Z_f$ | $T_e$ (eV) | $n_e$ ($cm^{-3}$) | $\alpha$ | $Z_f/Z_c^2$ | $I_e(k)/I_i(k)$ |
|---|---|---|---|---|---|
| 2 | 1 | $1\times10^{23}$ | 0.40 | 0.5 | 0.84 |
| 2 | 1 | $5\times10^{23}$ | 0.52 | 0.5 | 0.78 |
| 2 | 40 | $1\times10^{23}$ | 0.14 | 0.5 | 0.74 |
| 2 | 40 | $5\times10^{23}$ | 0.32 | 0.5 | 0.72 |
| 3 | 1 | $1\times10^{23}$ | 0.40 | 3.0 | 4.79 |
| 3 | 1 | $5\times10^{23}$ | 0.52 | 3.0 | 3.78 |
| 3 | 40 | $1\times10^{23}$ | 0.14 | 3.0 | 4.15 |
| 3 | 40 | $5\times10^{23}$ | 0.32 | 3.0 | 3.56 |

Table I for different values of $T_e$ and $n_e$. We see that the actual ratio $I_e(k)/I_i(k)$ depends slightly on both $T_e$ and $n_e$. The simple ratio $Z_f/Z_c^2$ underestimates the correct ratio $I_e(k)/I_i(k)$, since the parameter $\alpha$ is finite and the ionic form factor $f_I(k)\lesssim Z_c$ [$f_I(k)\sim1.6$ for $Z_f=2$ and $f_I(k)\sim0.83$ for $Z_f=3$]. Since in a scattering experiment, electron temperature and electron density can be extracted from a fit to the electron feature, Table I could be used to obtain the ionization state.

## IV. SUMMARY AND CONCLUDING REMARKS

In this paper, we have presented analytical expressions for the inelastic x-ray form factor that can be easily applied to interpreting scattering experiments in high density degenerate-to-hot plasmas. We have shown that x-ray Thomson scattering can be used as an effective diagnostic technique in plasmas produced under extreme conditions such as the ones occurring in ICF experiments or in the interiors of planets.

Although our calculation method is limited by the constraints of the RPA to coupling constants that are not too large, the solid density plasmas studied in this work lie within the range of validity of the RPA and extend from the full degenerate electron liquid to a classical electron gas. Such diverse conditions can thus be investigated with a different diagnostic technique, which will be useful, for example, to directly measure the electron temperature, ionization state, opacity, or electron conductivity from collisionality based on plasma resonance broadening, for EOS model validation. Synthetic spectra from low-$Z$ materials (e.g., beryllium) have been obtained and future comparison with experimental data will be necessary for a complete validation of x-ray Thomson scattering as a viable diagnostic method in low-$Z$ solid density plasmas.

## ACKNOWLEDGMENTS

We would like to acknowledge useful correspondence with Dr. J. Chihara. This work was performed under the auspices of the U.S. Department of Energy by the University of California Lawrence Livermore National Laboratory under Contract No. W-7405-ENG-48. We also acknowledge support from Laboratory Directed Research and Development Grant No. 02-ERD-13.

[1] S.H. Glenzer, *et al.*, Phys. Rev. Lett. **82**, 97 (1999).
[2] J. D. Lindl, *Inertial Confinement Fusion* (Springer-Verlag, New York, 1998).
[3] O.L. Landen, S.H. Glenzer, M.J. Edwards, R.W. Lee, G.W. Collins, R.C. Cauble, W.W. Hsing, and B.A. Hammel, J. Quant. Spectrosc. Radiat. Transf. **71**, 465 (2001).
[4] S. Ichimaru, Rev. Mod. Phys. **54**, 1017 (1982).
[5] R.L. Liboff, J. Appl. Phys. **56**, 2530 (1984).
[6] V.A. Bushuev and R.N. Kuz'min, Usp. Fiz. Nauk **122**, 81 (1977) [Sov. Phys. Usp. **20**, 406 (1977)].
[7] Y. Mizuno and Y. Ohmura, J. Phys. Soc. Jpn. **22**, 445 (1967).
[8] J. Chihara, J. Phys. F: Met. Phys. **17**, 295 (1987).
[9] J. Chihara, J. Phys.: Condens. Matter **12**, 231 (2000).
[10] D. Riley, N.C. Woolsey, D. McSherry, I. Weaver, A. Djaoui, and E. Nardi, Phys. Rev. Lett. **84**, 1704 (2000).
[11] S. Ichimaru, *Basic Principles of Plasma Physics* (Addison, Reading, MA, 1973).
[12] E.E. Salpeter, Phys. Rev. **120**, 1528 (1960).
[13] D.E. Evans and J. Katzenstein, Rep. Prog. Phys. **32**, 207 (1969).
[14] J.-P. Hansen and I. R. McDonald, *Theory of Simple Liquids* (Academic, London, 2000).
[15] E. Nardi, Phys. Rev. A **43**, 1977 (1991).
[16] E. Nardi, Z. Zinamon, D. Riley, and N.C. Woolsey, Phys. Rev. E **57**, 4693 (1998).
[17] Y.V. Arkhipov and A.E. Davletov, Phys. Lett. A **247**, 339 (1998).
[18] M. Baus and J.-P. Hansen, Phys. Rep. **59**, 1 (1980).
[19] F. Perrot and M.W.C. Dharma-Wardana, Phys. Rev. B **62**, 16 536 (2000).
[20] R. W. James, *The Optical Principles of the Diffraction of X-rays* (Ox Bow Press, Woodbridge, CT, 1962).
[21] L. Pauling and J. Sherman, Z. Kristallogr. **1**, 81 (1932).
[22] D. Waasmaier and A. Kirfel, Acta Crystallogr., Sect. A: Found. Crystallogr. **51**, 416 (1995).
[23] J.A. Anta and A.A. Louis, Phys. Rev. B **61**, 11 400 (2000).
[24] R. Kubo, J. Phys. Soc. Jpn. **12**, 570 (1957).
[25] L. D. Landau, E. M. Lifshitz, and L. P. Pitaevskii, *Physical Kinetics* (Pergamon, Oxford, 1995).
[26] D. Pines and D. Bohm, Phys. Rev. **85**, 338 (1952).
[27] D. Pines and P. Nozieres, *The Theory of Quantum Fluids* (Addison-Wesley, Redwood, CA, 1990).
[28] R. Cauble and D.B. Boercker, Phys. Rev. A **28**, 944 (1983).
[29] D.B. Boercker, R.W. Lee, and F.J. Rogers, J. Phys. B **16**, 3279 (1983).
[30] S. Ichimaru, S. Mitake, S. Tanaka, and X.-Z. Yan, Phys. Rev. A **32**, 1768 (1985).
[31] D.D. Carley, Phys. Rev. **131**, 1406 (1963).
[32] J.-P. Hansen, in *Molecular Dynamics Simulation of Statistical Mechanical Systems*, edited by G. Ciccotti and W. G. Hoover

(North-Holland, Amsterdam, 1986), Vol. 97.
[33] D. Pines, Rev. Mod. Phys. **28**, 184 (1956).
[34] P. Nozieres and D. Pines, Phys. Rev. **113**, 1254 (1959).
[35] P. Eisenberger, P.M. Platzman, and K.C. Pandy, Phys. Rev. Lett. **31**, 311 (1973).
[36] P. Eisenberger and P.M. Platzman, Phys. Rev. B **13**, 934 (1976).
[37] K. Awa, H. Yasuhara, and T. Asahi, Phys. Rev. B **25**, 3670 (1982).
[38] S. Ichimaru, *Statistical Plasma Physics* (Addison-Wesley, Reading, MA, 1991).
[39] J.W. DuMond and H.A. Kirkpatrick, Phys. Rev. **37**, 136 (1931).
[40] V.N. Tsytovich, Astropart. Phys. **5**, 185 (1996).
[41] S. Chandrasekhar, Phys. Rev. **34**, 1204 (1929).
[42] T. Suzuki, J. Phys. Soc. Jpn. **22**, 445 (1967).
[43] P.M. Platzman and N. Tzoar, Phys. Rev. **139**, A410 (1965).
[44] P. Eisenberger and P.M. Platzman, Phys. Rev. A **2**, 415 (1970).
[45] I.M. Band, M.B. Trzhaskovskaya, D.A. Verner, and D.G. Yakovlev, Astron. Astrophys. **267**, 237 (1990).
[46] A. Issolah, Y. Garreau, B. Levy, and G. Loupias, Phys. Rev. B **44**, 11 029 (1991).
[47] S.H. Glenzer, Bull. Am. Phys. Soc. **46**, 325 (2001).